Extreme Mechanics Letters 1 (2014) 42–46

Contents lists available at ScienceDirect

Extreme Mechanics Letters

journal homepage: www.elsevier.com/locate/eml

Mechanical and electrical numerical analysis of soft liquid-embedded deformation sensors analysis

Johannes T.B. Overvelde [a], Yiğit Mengüç [a,b,c], Panagiotis Polygerinos [a,b], Yunjie Wang [a], Zheng Wang [b,d], Conor J. Walsh [a,b], Robert J. Wood [a,b], Katia Bertoldi [a,*]

[a] School of Engineering and Applied Sciences (SEAS), Harvard University, Cambridge, MA, USA
[b] Wyss Institute for Biologically Inspired Engineering, Harvard University, Boston, MA, USA
[c] School of Mechanical, Industrial and Manufacturing Engineering (MIME), Oregon State University, Corvallis, OR, USA
[d] Department of Mechanical Engineering, The University of Hong Kong, Hong Kong

ARTICLE INFO

Article history:
Received 23 October 2014
Received in revised form 14 November 2014
Accepted 15 November 2014
Available online 4 December 2014

Keywords:
Finite element
Soft sensor
Liquid-embedded sensor
Large deformation

ABSTRACT

Soft sensors comprising a flexible matrix with embedded circuit elements can undergo large deformations while maintaining adequate performance. These devices have attracted considerable interest for their ability to be integrated with the human body and have enabled the design of skin-like health monitoring devices, sensing suits, and soft active orthotics. Numerical tools are needed to facilitate the development and optimization of these systems. In this letter, we introduce a 3D finite element-based numerical tool to simultaneously characterize the mechanical and electrical response of fluid-embedded soft sensors of arbitrary shape, subjected to any loading. First, we quantitatively verified the numerical approach by comparing simulation and experimental results of a dog-bone shaped sensor subjected to uniaxial stretch and local compression. Then, we demonstrate the power of the numerical tool by examining a number of different loading conditions. We expect this work will open the door for further design of complex and optimal soft sensors.

While engineering applications often use stiff and rigid materials, soft materials like elastomers enable the design of a new class of electronic devices that are flexible, stretchable, adaptive and can therefore be easily integrated with the human body [1–6]. These include highly conformable and extensible deformation sensors made from flexible substrates with embedded circuit elements, such as graphene sheets [7], nanotubes [8], interlocking nanofibres [9], serpentine patterned nanomembranes of Si [3,10,11], and conductive liquid micro channels [12–14].

A key feature of these sensors is their ability to reversibly stretch, bend, compress and twist to a great extent. Such deformations result in changes of the electrical resistance of the sensors, which are then used to determine the applied loading conditions. Therefore, the design of the next generation of soft sensors requires the development of numerical tools capable of predicting not only their mechanical performances [15,16], but also their electrical response. Such tools will enable the design of optimized sensors that are sensitive to desired loading conditions and also provide crucial insights into the working principles of these soft devices.

In this letter, we propose a 3D finite element-based numerical tool that predicts both the mechanical and electrical response of arbitrary shaped soft sensors subjected to any loading condition. In particular, we focus on sensors comprising an elastomeric matrix embedded with a network of channels filled with a conductive liquid [12–14], but the numerical approach can be easily extended to other types of soft sensors. The analyses are performed using the commercial finite element (FE) code Abaqus, which is an

* Corresponding author.
E-mail address: bertoldi@seas.harvard.edu (K. Bertoldi).

http://dx.doi.org/10.1016/j.eml.2014.11.003
2352-4316/

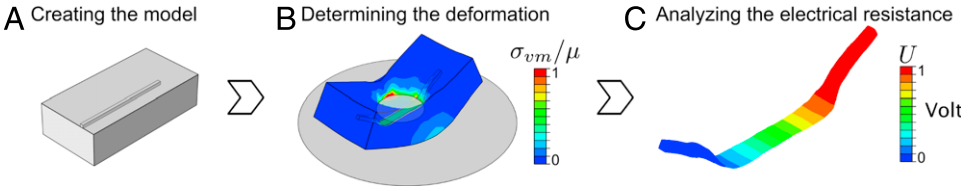

Fig. 1. The proposed FE-based numerical tool consists of three steps. (A) The model is created using CAD software and then meshed. (B) The deformation of the sensor is determined by using non-linear FE analysis, in which the contours show the normalized Von Mises stress σ_{vm}. (C) The resistance at different levels of deformation is obtained by performing a steady-state linear electrical conductivity analysis. The contours show the potential across the channel.

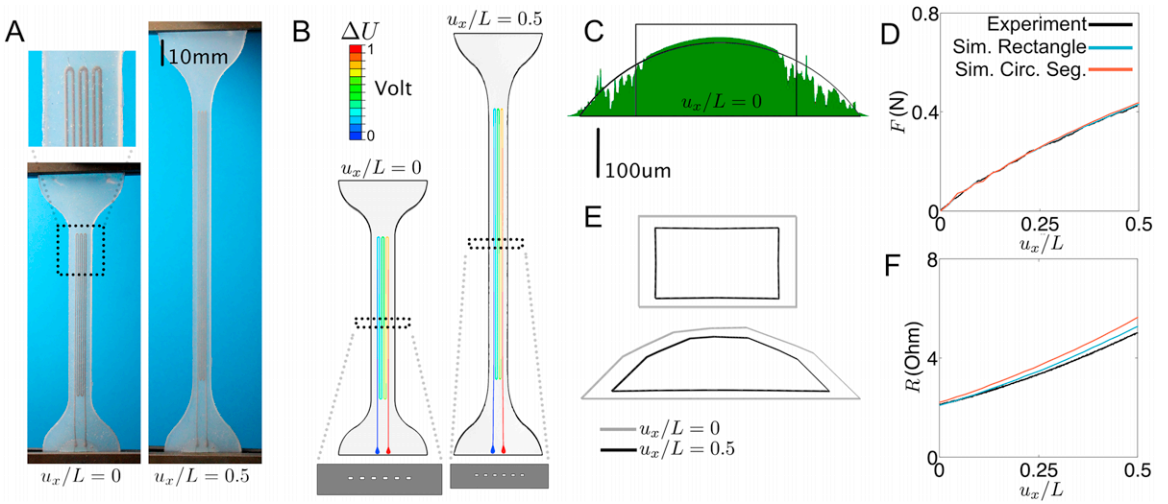

Fig. 2. Uniaxial extension of a dog-bone shaped soft sensor. (A) Experimental images of the undeformed ($u_x/L = 0$) and deformed ($u_x/L = 0.5$) sensor. (B) Numerical images of the undeformed ($u_x/L = 0$) and deformed ($u_x/L = 0.5$) sensor. The contours in the snapshot show the distribution of the electrical potential. (C) Cross-sectional profile measured with a laser interferometer (green) and cross-sections used in simulations. (D) Reaction force obtained in experiments and simulations as a function of the applied strain. (E) Cross-sections of the undeformed and deformed ($u_x/L = 0.5$) channels as predicted by the FE analysis. (F) Electrical resistance measured in experiments and simulations as a function of the applied strain.

attractive platform because it is well-known, widely available and particularly suitable for analyses involving large deformations. By making our code available online, we expect the proposed tool to be widely used and expanded to design more complex soft sensors with new and improved functions.

Our FE-based numerical tool consists of three steps, as indicated in Fig. 1 (the Abaqus script files and Matlab files used for our analysis are available online as Supporting Information):

Step A: Creating the model. A 3D model comprising both the flexible matrix and the circuit elements is first created using CAD software and then meshed. In particular, for the case of liquid-embedded soft sensors considered in this letter, the elastomeric matrix is meshed using linear tetrahedral elements (Abaqus element type *C3D4*), while a solid mesh of the channels is not created. In fact, only the surface mesh of the channel will be used to apply the pressure exerted by the fluid to the elastomer.

Step B: Determining the deformation. To determine the deformation of the sensor under specific loading conditions, a non-linear FE analysis is performed using the commercial package Abaqus/Explicit (v6.12). In the simulations, we fully account for contact between all faces of the model and ensure quasi-static conditions by monitoring the kinetic energy and introducing a small damping factor. For the case of liquid-embedded sensors investigated here, the response of the flexible matrix is captured using a nearly incompressible neo-Hookean material characterized by an initial shear modulus μ. Moreover, we consider the channels to be completely filled with a nearly incompressible fluid with bulk modulus $K = 100\mu$ and use the surface-based fluid cavity capability in Abaqus, so that the pressure applied by the fluid to the surface of the channel is determined from the cavity volume.

Step C: Analyzing the electrical resistance. To determine the electrical resistance of the deformed sensor, an isothermal steady-state linear electrical conductivity analysis (Abaqus step *Coupled thermal–electrical*) is performed on the deformed solid mesh of the circuit elements. Assuming the circuit elements are made of a material with electrical resistivity ρ, an electrical potential difference ΔU is applied between the two ends of the deformed circuit mesh and the dissipated work (W) over a time period of Δt is calculated. The electrical resistance of the channel (R) is then obtained as

$$R = \frac{\Delta U^2 \Delta t}{W}.$$

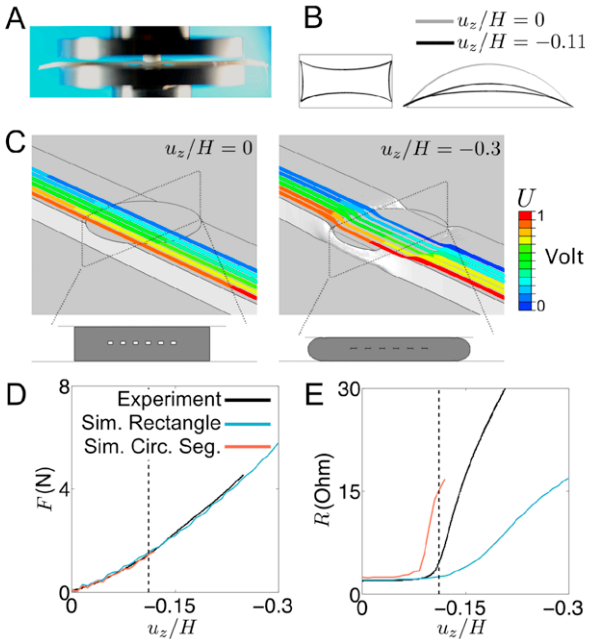

Fig. 3. Compression of a dog-bone shaped soft sensor using a circular punch. (A) Experimental set-up. (B) Cross-sections of the undeformed and deformed ($u_z/L = -0.11$) channels as predicted by the FE analysis. (C) Numerical images of the undeformed ($u_z/L = 0$) and deformed ($u_z/L = -0.3$) sensor. The contours in the snapshot show the distribution of the electrical potential. (D) Reaction force obtained in experiments and simulations as a function of the applied compressive strain. (E) Electrical resistance measured in experiments and simulations as a function of the applied compressive strain.

For the sake of convenience, in all our simulations we use $\Delta U = 1$V and $\Delta t = 1$s, so that $R = 1/W$. Note that for the specific case of liquid-embedded soft sensors, an additional meshing step is required, in which the deformed solid tetrahedral mesh of the channel is created starting from the deformed surface mesh obtained in Step B.

To validate our simulations, we focus on a dog-bone shaped soft sensor with a serpentine channel aligned along its length (see Fig. 2A), and compare the numerical predictions to experimental results for two different loading conditions: uniaxial tension and local compression. The sample is fabricated using silicone rubber (EcoFlex 0030, Smooth-On, Easton, PA, USA) and the channel is filled with the conductive liquid eutectic Gallium Indium (eGaIn) (Alfa Aesar, MA, USA) with resistivity $\rho = 29.4 \cdot 10^{-8}$ Ωm [17]. Details on the fabrication of the sample are reported in previous papers [12,18,19]. All experiments were conducted on a uniaxial materials testing machine (model 5544A, Instron Inc., MA, USA). To determine the electrical resistance R of the sensor, the sample was connected in series with a resistor with resistance R_{ref}. A potential difference ΔU_{ref} was applied to the entire system by a power supply, so that

$$R = R_{ref} \frac{\Delta U}{\Delta U_{ref} - \Delta U},$$

where ΔU is the potential difference between the two ends of the sensor's channel measured using a data acquisition card (BNC-2111, National Instruments Corp., TX, USA).

The dog-bone sample considered in this study has a central slender section of length $L = 50$ mm and a rectangular cross-section of 8 mm by 2 mm. Despite the fact that the sensor is designed to have an embedded channel with an overall length of 360 mm and a rectangular cross-section of 0.25 mm by 0.15 mm, we find that the actual cross-sectional shape of the channel is closer to that of a circular segment (see Fig. 2C). Therefore, in our simulations we consider two different cross-sectional shapes for the channel: (i) a rectangle of 0.3 mm by 0.172 mm and (ii) a circular segment with an angle of 111 degrees and a radius of 232 mm. Note that in both cases the area of the channel is equal to the experimentally measured value of 0.052 mm^2.

First, we load the sample uniaxially, as shown in Fig. 2A and B and Movies S1 and S2. From the mechanical response of the sensor, we find that the experimental measured stress–strain behavior can be fully captured modeling the elastomeric matrix as a neo-Hookean material with $\mu = 0.0221$ MPa (see Fig. 2D). As expected, we find that both the rectangular and circular segment channels deform in a similar manner and contract isotropically as the deformation increases (see Fig. 2E). The decrease in cross-sectional area of the channels results in an increase of the electrical resistance, which is captured in both experiments and simulations, as indicated in Fig. 2F. Remarkably, the numerical simulations, which do not require any fitting parameter, capture not only qualitatively but also quantitatively the evolution of R as a function of the applied deformation. Note that for this specific loading case our simulations indicate that both the electrical and mechanical response of the sensor are not affected by the shape of the channels, but only by their area (see Fig. 2F).

Next, we locally compress the sample in its center with a circular flat punch of radius 5 mm (see Fig. 3A and C and Movies S3, S4 and S5). For this loading condition the electrical response of the sensor is characterized by two distinct regimes (see Fig. 3E) [13,14,19]. For low values of

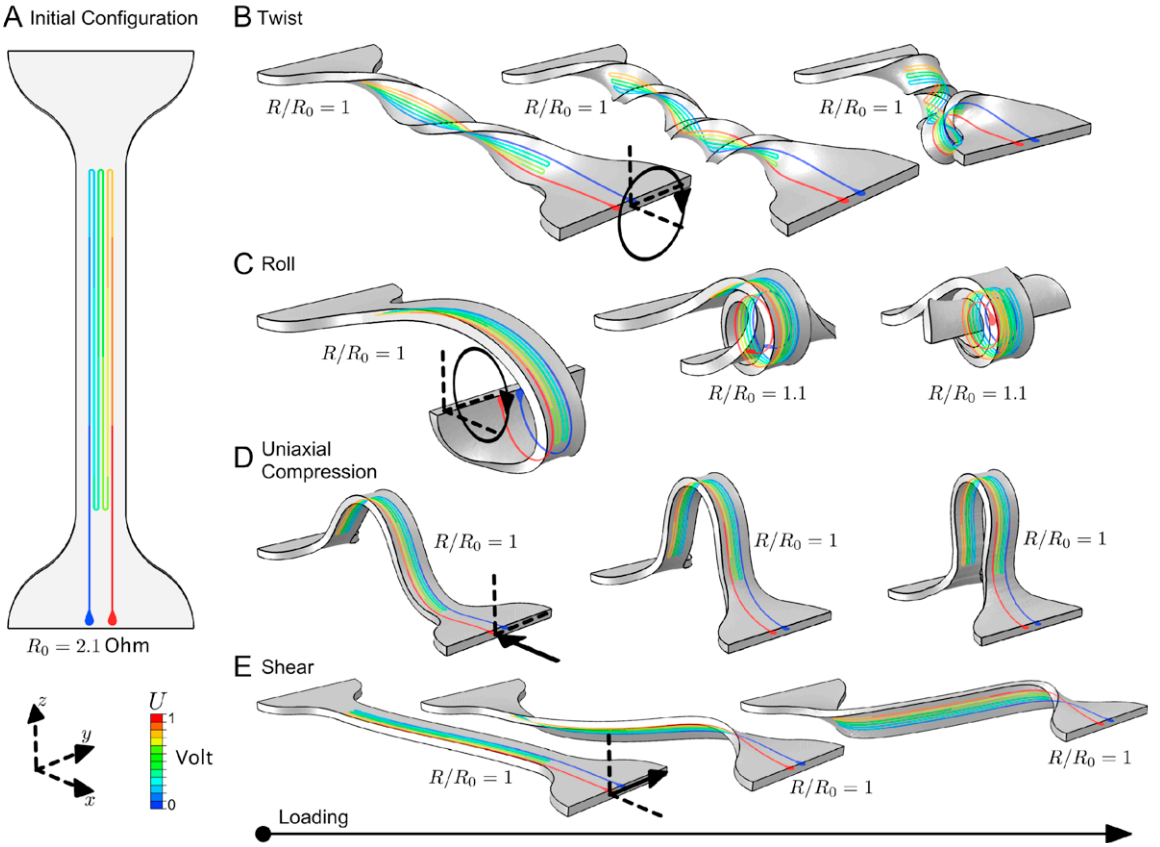

Fig. 4. Sensitivity of a dog-bone shaped soft sensor to various load cases. (A) Undeformed configuration. (B) Twist. (C) Roll. (D) Uniaxial compression in longitudinal direction. (E) Shear. The contours in the snapshot show the distribution of the electrical potential.

applied deformation ($u_z/H < -0.15$), the resistance R of the sensor is constant and not affected by the applied deformation. However, when the applied deformation is large enough to locally close the channel (see Fig. 3B), R increases rapidly. Remarkably, by using the same material parameters determined in our previous analysis, the numerical simulations exactly capture the experimentally measured mechanical response (see Fig. 3D). Furthermore, as shown in Fig. 3E, the simulations also correctly capture the electrical response of the sensors and reveal that the level of applied deformation at which R starts to rapidly increase is highly sensitive to the cross-sectional shape of the channel. Such sensitivity has been previously shown experimentally [12,20] and is dictated by the fact that the load required to locally close the channel is highly affected by its shape. In particular, we find that the circular segment cross-section completely closes for smaller values of applied strain (Fig. 3B), resulting in a sensor that is more sensitive to local compression.

Now that we have verified the robustness of our numerical tool, we use it to characterize the sensitivity of our sensor to different loading conditions. In particular, we consider four different loading cases: (i) we twist the sensor by rotating one side around the x-axis by a 6π angle as shown in Fig. 4B and Movies S6; (ii) we roll the sensor by rotating one of its ends around the y-axis by a 4π angle (see Fig. 4C and Movie S7); (iii) we compress the sensor uniaxially along the x-axis by $u_x/L = -0.5$ (Fig. 4D and Movie S8); (iv) we shear the sensor by displacing one of the ends along the y-axis by $u_y/L = 0.5$ (Fig. 4E and Movie S9). Note that for the loading cases (i), (ii) and (iv) the sensor is free to move in the z-direction, so that it does not stretch uniaxially. Surprisingly, although in all these simulations the channels are drastically deformed, the electrical resistance of the sensor remains nearly unaltered, i.e. $R/R_0 \sim 1$.

Therefore, our simulations indicate that this dog-bone sensor is extremely well suited for applications in which uniaxial tensile strain applied along the longitudinal direction needs to be monitored. In fact, much higher forces are required to make the sensor sensitive to local compression in the z-direction, i.e. 0.4N and 2N need to be applied to increase the electrical resistance by 100% under uniaxial extension and local compression, respectively. Moreover, all other simulated loading conditions are found to leave the electrical resistance unchanged even for extreme values of applied deformation.

In summary, we introduced an effective finite element procedure to characterize simultaneously the mechanical and electrical response of soft sensors of any shape subjected to arbitrarily loading conditions. The accuracy and robustness of the proposed numerical method was verified by comparing the numerical and experimental results for the case of a dog-bone shaped soft sensor with a serpentine channel aligned along its length. The simulations not only

quantitatively capture both the mechanical and electrical response of the sensor, but also enable us to determine the role played by the shape of the cross-section and different loading conditions, facilitating the design of sensors which are only sensitive to specific loads.

This work opens the door for further simulation-based studies of soft sensors with complex microstructures, which would otherwise be intractable to address analytically or experimentally. In particular, the proposed numerical tool may serve as a platform to accelerate the design of devices such as embedded 3D printed circuits [21], liquid metal pumps [22], and health-monitoring devices [3,8,19,23].

Acknowledgments

This work was supported by the Materials Research Science and Engineering Center under NSF Award No. DMR-0820484. K.B. also acknowledges support from the National Science Foundation (CMMI-1149456-CAREER) and the Wyss institute through the Seed Grant Program.

Appendix A. Supplementary data

Supplementary material related to this article can be found online at http://dx.doi.org/10.1016/j.eml.2014.11.003.

References

[1] J.A. Rogers, Y. Huang, A curvy, stretchy future for electronics, Proc. Natl. Acad. Sci. 106 (27) (2009) 10875–10876.
[2] J.A. Rogers, T. Someya, Y. Huang, Materials and mechanics for stretchable electronics, Science 327 (5973) (2010) 1603–1607.
[3] L. Xu, S.R. Gutbrod, A.P. Bonifas, Y. Su, M.S. Sulkin, N. Lu, H.-J. Chung, K.-I. Jang, Z. Liu, M. Ying, C. Lu, R.C. Webb, J.-S. Kim, J.I. Laughner, H. Cheng, Y. Liu, A. Ameen, J.-W. Jeong, G.-T. Kim, Y. Huang, I.R. Efimov, J.A. Rogers, 3d multifunctional integumentary membranes for spatiotemporal cardiac measurements and stimulation across the entire epicardium, Nature Commun., 5.
[4] C. Yu, Y. Li, X. Zhang, X. Huang, V. Malyarchuk, S. Wang, Y. Shi, L. Gao, Y. Su, Y. Zhang, H. Xu, R.T. Hanlon, Y. Huang, J.A. Rogers, Adaptive optoelectronic camouflage systems with designs inspired by cephalopod skins, Proc. Natl. Acad. Sci. 111 (36) (2014) 12998–13003.
[5] J.-H. So, J. Thelen, A. Qusba, G.J. Hayes, G. Lazzi, M.D. Dickey, Reversibly deformable and mechanically tunable fluidic antennas, Adv. Funct. Mater. 19 (22) (2009) 3632–3637.
[6] C. Keplinger, J.-Y. Sun, C.C. Foo, P. Rothemund, G.M. Whitesides, Z. Suo, Stretchable, transparent, ionic conductors, Science 341 (6149) (2013) 984–987.
[7] Y. Wang, R. Yang, Z. Shi, L. Zhang, D. Shi, E. Wang, G. Zhang, Super-elastic graphene ripples for flexible strain sensors, ACS Nano 5 (5) (2011) 3645–3650.
[8] T. Yamada, Y. Hayamizu, Y. Yamamoto, Y. Yomogida, A. Izadi-Najafabadi, D.N. Futaba, K. Hata, A stretchable carbon nanotube strain sensor for human-motion detection, Nature Nano 6 (5) (2011) 296–301.
[9] C. Pang, G.-Y. Lee, T.-i. Kim, S.M. Kim, H.N. Kim, S.-H. Ahn, K.-Y. Suh, A flexible and highly sensitive strain-gauge sensor using reversible interlocking of nanofibres, Nature Mater. 11 (9) (2012) 795–801.
[10] D.-H. Kim, N. Lu, R. Ma, Y.-S. Kim, R.-H. Kim, S. Wang, J. Wu, S.M. Won, H. Tao, A. Islam, K.J. Yu, T.-i. Kim, R. Chowdhury, M. Ying, L. Xu, M. Li, H.-J. Chung, H. Keum, M. McCormick, P. Liu, Y.-W. Zhang, F.G. Omenetto, Y. Huang, T. Coleman, J.A. Rogers, Epidermal electronics, Science 333 (6044) (2011) 838–843.
[11] D. Son, J. Lee, S. Qiao, R. Ghaffari, J. Kim, J.E. Lee, C. Song, S.J. Kim, D.J. Lee, S.W. Jun, S. Yang, M. Park, J. Shin, K. Do, M. Lee, K. Kang, C.S. Hwang, N. Lu, T. Hyeon, D.-H. Kim, Multifunctional wearable devices for diagnosis and therapy of movement disorders, Nature Nano 9 (5) (2014) 397–404.
[12] Y.L. Park, C. Majidi, R. Kramer, P. Berard, R.J. Wood, Hyperelastic pressure sensing with a liquid-embedded elastomer, J. Micromech. Microeng. 20 (12).
[13] Y.L. Park, B.R. Chen, R.J. Wood, Design and fabrication of soft artificial skin using embedded microchannels and liquid conductors, IEEE Sens. J. 12 (8) (2012) 2711–2718.
[14] D.M. Vogt, Y.L. Park, R.J. Wood, Design and characterization of a soft multi-axis force sensor using embedded microfluidic channels, IEEE Sens. J. 13 (10) (2013) 4056–4064.
[15] Y. Su, Z. Liu, S. Kim, J. Wu, Y. Huang, J.A. Rogers, Mechanics of stretchable electronics with high fill factors, Int. J. Solids Struct. 49 (23–24) (2012) 3416–3421.
[16] Y. Zhang, H. Fu, S. Xu, J.A. Fan, K.-C. Hwang, J. Jiang, J.A. Rogers, Y. Huang, A hierarchical computational model for stretchable interconnects with fractal-inspired designs, J. Mech. Phys. Solids 72 (0) (2014) 115–130.
[17] M.D. Dickey, R.C. Chiechi, R.J. Larsen, E.A. Weiss, D.A. Weitz, G.M. Whitesides, Eutectic gallium-indium (EGaIn): A liquid metal alloy for the formation of stable structures in microchannels at room temperature, Adv. Funct. Mater. 18 (7) (2008) 1097–1104.
[18] Y. Mengüç, Y.-L. Park, E. Martinez-Villalpando, P. Aubin, M. Zisook, L. Stirling, R.J. Wood, C.J. Walsh, Soft wearable motion sensing suit for lower limb biomechanics measurements, IEEE Internat. Conf. Robot. Automation ICRA (2013) 5309–5316.
[19] Y. Mengüç, Y.-L. Park, H. Pei, D.M. Vogt, P. Aubin, E. Winchell, L. Fluke, L. Stirling, R.J. Wood, C.J. Walsh, Wearable soft sensing suit for human gait measurement, Int. J. Robot. Res..
[20] Y.L. Park, D. Tepayotl-Ramirez, R.J. Wood, C. Majidi, Influence of cross-sectional geometry on the sensitivity and hysteresis of liquid-phase electronic pressure sensors, Appl. Phys. Lett., 101, 19.
[21] J.T. Muth, D.M. Vogt, R.L. Truby, Y. Mengüç, D.B. Kolesky, R.J. Wood, J.A. Lewis, Embedded 3d printing of strain sensors within highly stretchable elastomers, Advanced Mater. 26 (36) (2014) 6307–6312.
[22] S.-Y. Tang, K. Khoshmanesh, V. Sivan, P. Petersen, A.P. O'Mullane, D. Abbott, A. Mitchell, K. Kalantar-zadeh, Liquid metal enabled pump, Proc. Natl. Acad. Sci. 111 (9) (2014) 3304–3309.
[23] C. Wang, W. Zheng, Z. Yue, C.O. Too, G.G. Wallace, Buckled, stretchable polypyrrole electrodes for battery applications, Advanced Materials 23 (31) (2011) 3580–3584.